Investigation of an Explicit, Residual-Based, a Posteriori Error Indicator for the Adaptive Finite Element Analysis of Waveguide Structures

Matthys M. Botha and David B. Davidson

Department of Electrical and Electronic Engineering, University of Stellenbosch, Private Bag X1, Matieland 7602, Stellenbosch, South Africa

***Abstract*— The performance of an explicit, residual-based, a posteriori error indicator for directing a single level p-refinement of the finite element method, electromagnetic analysis of multi-port waveguide structures is evaluated experimentally by considering three different structures. The error indicator consists of a linear combination of element volume and element face residuals. It is found that the indicator is generally very effective in identifying elements that need to be refined. It is also found that the relative weighting of the volume and face residual contributions to the error indicator plays an important role in its performance.**

I. Introduction

The Finite Element Method (FEM) can be used very effectively in the analysis of waveguide structures. References [1], [2], [3], [4] represent some examples of the driven problem and [5], [6] represent some examples of the eigenvalue problem. There are fundamental differences between the driven- and eigenvalue problems. The eigenvalue problem is typically a 2D analysis of the waveguide transverse plane with the purpose of finding the modal field distributions and cutoff frequencies, whereas the driven problem can be in 2D (see [4]), but is generally constructed in 3D (see [1], [2], [3]). The driven problem needs to include the waveguide port(s) within the variational formulation as an inhomogeneous, Dirichlet boundary condition (the voltage-current approach, see [4]) or as a special type of Neumann boundary condition (the incident-reflected approach, see [1], [2], [3]).

In this paper we will use curl-conforming, vector elements to analyze 3D, multi-port, inhomogeneously filled, waveguide structures at specific frequencies (a driven problem), using Neumann boundary conditions to model the ports. These elements posses fundamental advantages over scalar elements, as discussed in numerous publications [6], [7], [8], [9]. The waveguide port variational boundary value problem and the resulting FEM is discussed in Section II.

The main contribution of this paper is the experimental performance evaluation of an explicit, residual-based, a posteriori error indicator when used to direct a single level p-refinement. Error indicators are commonly used for refining finite element discretizations in an iterative manner.

The error indicator is presented in Section III and is a proper bound on an approximate energy norm. It can be derived from the waveguide port variational boundary value problem, as shown in [10], [11]. It is explicit in nature and based on volume and trace residuals. The indicator is of the same general form as a residual-based indicator presented in [12, eq.(3.18)] for the general, scalar, elliptic boundary value problem case, bounding the proper energy norm. There are clearly some important differences between our indicator and the one in [12], but these will not be discussed further. Other examples of indicators, similar to the one used here, can be found in the literature. Reference [6, Appendix G] presents an explicit, residual-based indicator tailored to the vector wave equation, but it does not incorporate the waveguide port formulation that we employ and only deals with 2D problems. Reference [13] presents an explicit, residual-based estimator for 3D, electrostatic problems. Explicit, residual-based indicators that bound the L^2 norm of the error as opposed to the (approximate) energy norm, can also be derived — see [12], [14] for the scalar elliptic case and [15] for the Maxwell system case where an open boundary, hybrid FEM is considered, employing spherical harmonics, similar in some respect to the unimoment method [16].

Ideally, one would like to investigate the performance of an error indicator experimentally by considering problems with analytical solutions. Unfortunately, very few such problems are available for the type of multi-port waveguide structures that are considered here. Therefore, we resorted to considering the errors with respect to higher order solutions as a measure of the true performance. This still is of great practical value, since the maximum available order solution represents the closest possible approximation of the true solution for a given discretization, in any case. We restrict ourselves to two elements of different order that are widely used: the Constant Tangential/Linear Normal (CT/LN) and Linear Tangential/Quadratic Normal (LT/QN) elements [9]. Section IV describes the investigative procedure followed. In Sections V, VI and VII, investigative results of three different waveguide port structures are presented and discussed.

We end by drawing some overall conclusions in light of all the available results.

In this paper, the subscript w will indicate entities associated with the feeding waveguides and/or their corresponding port apertures.

1054-4887 ' 2006 ACES

II. The waveguide, finite element formulation

The electric field, vector wave equation, boundary value problem on the volume Ω, is as follows [1]:

$$\left\{\begin{aligned} \nabla\times\frac{1}{\mu_r}\nabla\times\mathbf{E}-k_0^2\epsilon_r\mathbf{E} &= -jk_0Z_0\mathbf{J} && \text{on } \Omega,\\ \hat{n}\times\mathbf{E} &= 0 && \text{on } \Gamma_D,\\ \hat{n}\times\nabla\times\mathbf{E} &= \mathbf{N} && \text{on } \Gamma_N,\end{aligned}\right. \tag{1}$$

where Γ_D represents the homogeneous, Dirichlet boundary and Γ_N represents the inhomogeneous, Neumann boundary. $\mathbf{J}$ represents an impressed current distribution and $\mathbf{N}$ represents a general Neumann boundary condition.

The electric field, vector wave equation, boundary value problem can be expressed as a variational boundary value problem [11], yielding

$$\left\{\begin{aligned} &\int_\Omega\left\{\frac{1}{\mu_r}\nabla\times\mathbf{E}\cdot\nabla\times\mathbf{W}-k_0^2\epsilon_r\mathbf{E}\cdot\mathbf{W}\right\}dV\\ &=-\int_{\Gamma_N}\frac{1}{\mu_r}\mathbf{N}\cdot\mathbf{W}\,dS-jk_0Z_0\int_\Omega\mathbf{J}\cdot\mathbf{W}\,dV\\ &\qquad\forall\ \mathbf{W}\in W;\quad \mathbf{E}\in W\end{aligned}\right. \tag{2}$$

with

$$W=\{\mathbf{a}\in H(\text{curl},\Omega)\mid\hat{n}\times\mathbf{a}=0\text{ on }\Gamma_D\}\,. \tag{3}$$

Dominant, TE_{10} mode modeling of a waveguide port is included in the variational boundary value problem via a Neumann boundary condition at the port aperture S_w, as described in [1]. The resulting variational boundary value problem is as follows:

$$\left\{\begin{aligned} &\int_\Omega\left\{\frac{1}{\mu_r}\nabla\times\mathbf{E}\cdot\nabla\times\mathbf{W}-k_0^2\epsilon_r\mathbf{E}\cdot\mathbf{W}\right\}dV\\ &\quad+\frac{jk_w}{\mu_{rw}}\int_{S_w}(\hat{n}\times\mathbf{E})\cdot(\hat{n}\times\mathbf{W})\,dS\\ &\quad=\frac{2jk_w}{\mu_{rw}}\int_{S_w}(\hat{n}\times\mathbf{E}_w^{\text{inc}})\cdot(\hat{n}\times\mathbf{W})\,dS\\ &\qquad\forall\ \mathbf{W}\in W;\quad \mathbf{E}\in W.\end{aligned}\right. \tag{4}$$

Note that the impressed, electric current source term was dropped in equation (4), since no such sources will be present in the waveguide problems considered here.

$\mathbf{E}_w^{\text{inc}}$ and k_w represent the incident, TE_{10} wave at the port and the feeding waveguide, TE_{10} mode propagation constant, respectively. They are defined in terms of the local port coordinate system shown in Figure 1, as follows [17]:

$$\mathbf{E}_w^{\text{inc}}=E_w^{\text{inc}}\sin\left(\frac{\pi x}{a}\right)\hat{y}. \tag{5}$$

$$k_w=\sqrt{k_0^2-\left(\frac{\pi}{a}\right)^2}. \tag{6}$$

A finite element discretization is employed in order to solve equation (4) in an approximate manner. The electric field is represented as

$$\mathbf{E}_h=\sum_{i=1}^{N_F}E_i\mathbf{N}_i, \tag{7}$$

with the E_i representing the unknown degrees of freedom and the $\mathbf{N}_i$ representing the basis functions. By choosing the testing functions equal to the basis functions, equation (4) leads to a symmetric matrix equation $[A]\{E\}=\{b\}$ in terms of the degrees of freedom.

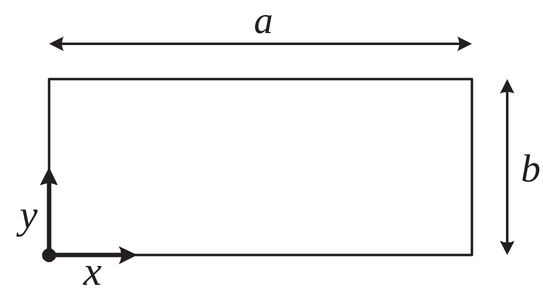

Fig. 1. Waveguide aperture. Definitions of the local coordinate system and dimensions.

Curl-conforming, hierarchal, vector basis functions of mixed order are used [9]. Since the elements are of mixed order, they model the unknown field and its curl to the same polynomial degree, with the least possible degrees of freedom [18]. Note that both of these quantities play roles of equal importance in equation (4). Normal field continuity is not enforced by curl-conforming elements; the associated benefits are outlined in [7]. The elements are hierarchal, which means that elements of different polynomial order can easily be used within the same mesh.

In the rest of this paper, the hierarchal property of the elements is of great importance, since CT/LN ($\text{H}_0(\text{curl})$) and LT/QN ($\text{H}_1(\text{curl})$) elements are used together. The definitions of the basis functions used, can be found in [19].

III. The waveguide, explicit, residual-based, error indicator

Define the error field as

$$\mathbf{e}_h=\mathbf{E}-\mathbf{E}_h. \tag{8}$$

Define K as a single, elemental volume of the mesh and define f as a single, facial area of the mesh, with N_K as the number of elements in the mesh and N_f as the number of faces in the mesh. Further define

$$h_{K(i)}=\text{diam}(K_i), \tag{9}$$

$$h_{f(m)}=\begin{cases}\max\left\{\text{diam}(K^{(1)}),\text{diam}(K^{(2)})\right\} & \text{internal face},\\ \text{diam}(K^{(1)}) & \text{boundary face},\end{cases} \tag{10}$$

where the superscripts (1) and (2) indicate the two elements sharing the face concerned and $\text{diam}(K)$ indicates the diameter (maximum dimension) of element K.

The following explicit, residual-based, error bound can be derived for the discretized, waveguide variational boundary value problem of equation (4) [10], [11]:

$$\begin{aligned}\|\mathbf{e}_h\|^2_{E^a(\Omega)}\ \le\ & C_V\sum_{i=1}^{N_K}h^2_{K(i)}\|\mathbf{R}_V\|^2_{L^2(K_i)}\\ &+C_f\sum_{m=1}^{N_f}h_{f(m)}\|\mathbf{R}_f\|^2_{L^2(f_m)},\end{aligned} \tag{11}$$

with the approximate energy norm defined as

$$\begin{aligned}\|\mathbf{a}\|_{E^a(\Omega)} &\equiv \left[\sum_{i=1}^{N_K} |\mathbf{a}|^2_{(H^1(K_i))^3}\right]^{-\frac{1}{2}} \\ &\cdot \left| \int_\Omega \left\{ \frac{1}{\mu_r} \nabla \times \mathbf{a} \cdot \nabla \times \mathbf{a} - k_0^2 \epsilon_r \mathbf{a} \cdot \mathbf{a} \right\} dV \right. \\ &\left. + \frac{jk_w}{\mu_{rw}} \int_{S_w} (\hat{n} \times \mathbf{a}) \cdot (\hat{n} \times \mathbf{a})\, dS \right| \qquad (12)\end{aligned}$$

where $|\mathbf{a}|_{(H^1(K))^3}$ designates the Sobolev semi-norm of order 1, on elemental volume K [20]. The volume and face residuals in equation (11) are defined as

$$\mathbf{R}_V = -\nabla \times \frac{1}{\mu_r} \nabla \times \mathbf{E}_h + k_0^2 \epsilon_r \mathbf{E}_h \quad \text{in } K_i;\ i = 1, ..., N_K. \qquad (13)$$

$$\mathbf{R}_f = \begin{cases} \hat{n}^{(12)} \times \left[\frac{1}{\mu_r^{(1)}} \nabla \times \mathbf{E}_h^{(1)} - \frac{1}{\mu_r^{(2)}} \nabla \times \mathbf{E}_h^{(2)} \right] \\ \qquad \text{on } f_m \setminus S_w;\ m = 1, ..., N_f \\ \frac{1}{\mu_r} \hat{n} \times \nabla \times \mathbf{E}_h - \frac{jk_w}{\mu_{rw}} \hat{n} \times \left[\hat{n} \times \left(2\mathbf{E}_w^{\text{inc}} - \mathbf{E}_h \right) \right] \\ \qquad \text{on } f_m \cap S_w;\ m = 1, ..., N_f. \end{cases} \qquad (14)$$

It is clear that $\|\mathbf{e}_h\|_{E^a(\Omega)}$ is not a proper norm of the error field, because it does not conform to the well known specifications of a proper norm [21], since $\|\mathbf{e}_h\|_{E^a(\Omega)} = 0 \not\Rightarrow \mathbf{e}_h = 0$. However, $\mathbf{e}_h = 0 \Rightarrow \|\mathbf{e}_h\|_{E^a(\Omega)} = 0$ and one can further observe that the residuals (and therefore the RHS of equation (11)) will go to zero when $\mathbf{E}_h$ satisfies the vector wave equation and the Maxwell continuity conditions [17]. Therefore: the RHS of equation (11) can reliably indicate the presence of an error, but not the absence thereof. This is not ideal, but it will be shown to be quite useful.

Equation (11) can be rewritten in terms of elemental contributions to the bound on $\|\mathbf{e}_h\|^2_{E^a(\Omega)}$. It is assumed that the facial contributions are shared equally between elements. The boundary face contributions are also scaled by $1/2$ even though they are not shared, since they represent the same Maxwell continuity condition as the internal face residuals and should therefore be treated in the same way. Equation (11) becomes a summation of elemental error indicators:

$$\begin{aligned}\|\mathbf{e}_h\|^2_{E^a(\Omega)} &\leq \sum_{i=1}^{N_K} \Big(C_V h^2_{K(i)} \|\mathbf{R}_V\|^2_{L^2(K_i)} \\ &+ \frac{1}{2} C_f \sum_{f_m \subset \partial K_i} h_{f(m)} \|\mathbf{R}_f\|^2_{L^2(f_m)} \Big). \qquad (15)\end{aligned}$$

The unknown constants C_V and C_f in equation (15) can be replaced with two new constants, C and α, resulting in

$$\begin{aligned}\|\mathbf{e}_h\|^2_{E^a(\Omega)} &\leq C \sum_{i=1}^{N_K} \Big(\alpha h^2_{K(i)} \|\mathbf{R}_V\|^2_{L^2(K_i)} \\ &+ \frac{1}{2}(1-\alpha) \sum_{f_m \subset \partial K_i} h_{f(m)} \|\mathbf{R}_f\|^2_{L^2(f_m)} \Big), \qquad (16)\end{aligned}$$

with

$$0 \leq \alpha \leq 1. \qquad (17)$$

The value α clearly represents the relative contributions of the volume- and facial residuals to the elemental indicators. The effect of this parameter on the indicator performance will be studied in the subsequent sections.

IV. Investigative procedure

This section describes a procedure for evaluating the effect of the parameter α on the performance of the error indicator of equation (16), for a specific problem and at a specific frequency.

After an all-CT/LN solution, the following elemental error indicator is calculated for every element K_i, $i = 1, .., N_K$, with fixed α:

$$\alpha h^2_{K(i)} \|\mathbf{R}_V\|^2_{L^2(K_i)} + \frac{1}{2}(1-\alpha) \sum_{f_m \subset \partial K_i} h_{f(m)} \|\mathbf{R}_f\|^2_{L^2(f_m)}. \qquad (18)$$

The problem is then re-solved, but with a percentage of elements with the highest error indicator values upgraded to LT/QN elements. Since the quality of the upgraded solution must lie between that of an all-CT/LN- and an all-LT/QN solution, the relative solution quality error ϵ_Q, measured in terms of the reflection coefficient S_{11}, is defined as follows:

$$\epsilon_Q = \left| \frac{S_{11} - S_{11}^{\text{LT/QN}}}{S_{11}^{\text{LT/QN}}} \right|. \qquad (19)$$

The value ϵ_Q is called relative, since it is a measure of the solution quality error $\left| S_{11} - S_{11}^{\text{LT/QN}} \right|$, *relative* to the magnitude of the highest order solution, $\left| S_{11}^{\text{LT/QN}} \right|$.

Various ϵ_Q values are obtained for the current value of α, by changing the percentage of elements that are upgraded to LT/QN. In all graphs to be presented, the following set of percentages were used: 0.0%, 2.5%, 5.0%, 7.5%, 10.0%, 12.5% and 100.0%. This defines a curve of ϵ_Q as a function of the number of degrees of freedom. A set of such curves is generated at a given frequency point by considering a range of α values and will henceforth be referred to as a *performance graph*. On every performance graph a curve denoted "Random" is included for reference purposes. These curves were generated by upgrading randomly selected elements. Considering a specific problem, a distinct performance graph can be generated by the above described procedure, at any frequency.

As an example, consider Figure 4, the performance graph of a waveguide through problem at $f = 8.5$ GHz, to be discussed in Section V. The first cluster of data points, around 1500 degrees of freedom, represents an upgrade of 2.5% of the elements. Following clusters represent the other upgrade percentages used. These clusters can be quite spread out, since the upgrading of two neighbouring elements results in fewer additional degrees of freedom than the upgrading of two free-standing elements (upgrading an element necessitates the partial upgrading of its neighbours in order to maintain tangential field continuity). At a specific upgrade percentage, the number of degrees of freedom depends on the element selection scheme and will thus vary with α. The number of degrees of freedom (rather than the upgrade percentage) was chosen as the x-axis variable of the performance graphs, since it is a good indicator of relative computational effort.

Various performance graphs of various problems will be considered in order to ascertain whether a pattern is present.

V. RESULTS: PERFORMANCE GRAPHS OF A WAVEGUIDE THROUGH PROBLEM

This section considers a waveguide through problem. The geometry of the problem is a straight, empty length of standard X-band waveguide. Figure 2 shows the finite element mesh. Figure 3 compares the reflection coefficient values obtained with all-CT/LN- and all-LT/QN elements, with the analytical solution, showing that the LT/QN result is indeed an improvement upon the CT/LN result.

Performance graphs for this structure were calculated at $f = 8.5$ GHz, $f = 9.5$ GHz, and $f = 10.5$ GHz. In this case the solution quality error was not divided by $\left|S_{11}^{\mathrm{LT/QN}}\right|$, because the true reflection coefficient is zero. Figures 4, 5 and 6 show the performance graphs.

There seems to be no consistent tendency in the performance graphs. The error indicator performance is generally poor. We propose the following reason for this behaviour:

The actual field possesses no variation in amplitude along the guide length, only a sinusoidal variation in phase. In the transverse plane there is only a sinusoidal, amplitude variation in the local (see Figure 1) x-direction. Since the actual field variations are clearly very slow and uniform throughout the whole structure, the actual error distribution is relatively flat, compared to the other problems considered in this paper. Thus, one actually needs to upgrade the mesh uniformly, rather than selectively, for optimal error reduction.

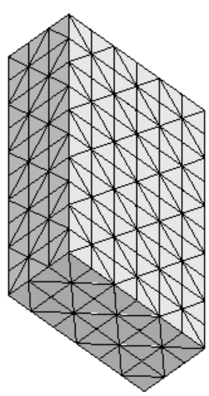

Fig. 2. Finite element mesh of the waveguide through problem. 1194 elements, average edge length is 4.5 mm. The ports are transverse to the longest dimension of the structure. The transverse waveguide geometry is as shown in Figure 1, with $a = 22.86$ mm and $b = 10.16$ mm.

VI. RESULTS: PERFORMANCE GRAPHS OF A WAVEGUIDE IRIS PROBLEM

This section considers a waveguide iris problem. The geometry of the problem is a straight, empty length of X-band waveguide, except for an infinitely thin PEC iris located at its center. Figure 7 shows the iris geometry. Figure 8 shows the finite element mesh. Figure 9 compares the reflection coefficient values obtained with all-CT/LN- and all-LT/QN elements, with an approximate, analytical result by Marcuvitz [22], showing that the LT/QN result is indeed an improvement upon the CT/LN result. Marcuvitz's results are lumped-element circuit models; in [3] the procedure required to obtain s-parameters from these was outlined.

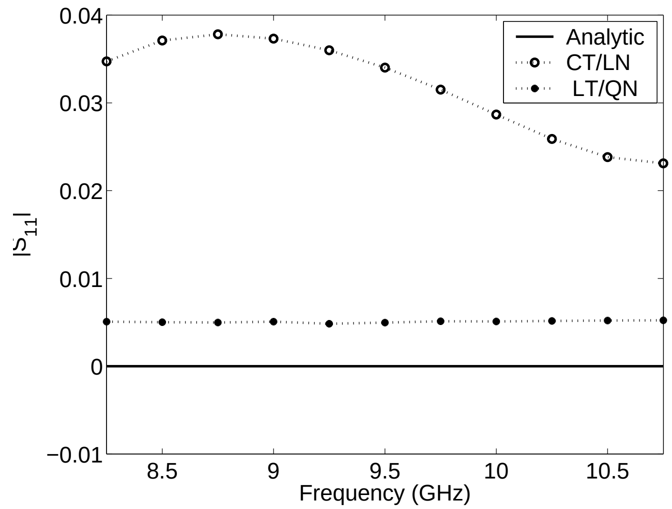

Fig. 3. S_{11} vs. frequency of the waveguide through problem.

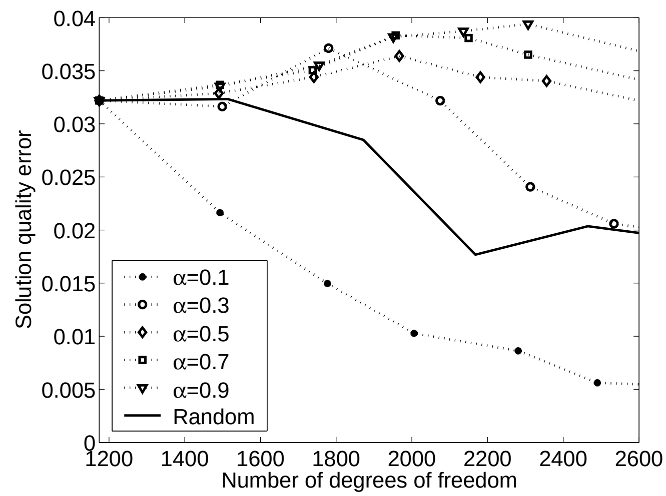

Fig. 4. Solution quality error vs. number of degrees of freedom for the waveguide through problem at $f = 8.5$ GHz. The all LT/QN number of degrees of freedom, at which the solution quality error is zero for all α, is 6836.

Performance graphs for this structure were calculated at $f = 8.5\,$GHz, $f = 9.5\,$GHz and $f = 10.5\,$GHz. Figures 10, 11 and 12 show the performance graphs.

Observe the following tendency in the performance graphs: when considering only a small increase in the number of degrees of freedom ($\leq 2.5\%$ upgraded elements), a dominant surface contribution leads to superior results ($\alpha < 0.5$), but if one intends to upgrade $\geq 5\%$ of the elements, a value of

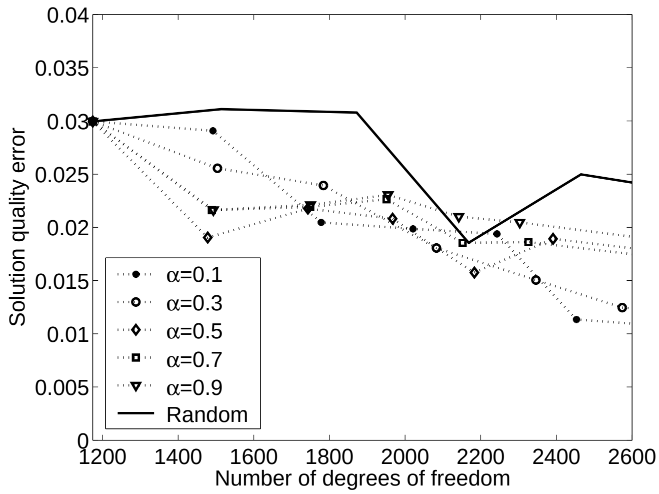

Fig. 5. Solution quality error vs. number of degrees of freedom for the waveguide through problem at $f = 9.5$ GHz. The all LT/QN number of degrees of freedom, at which the solution quality error is zero for all α, is 6836.

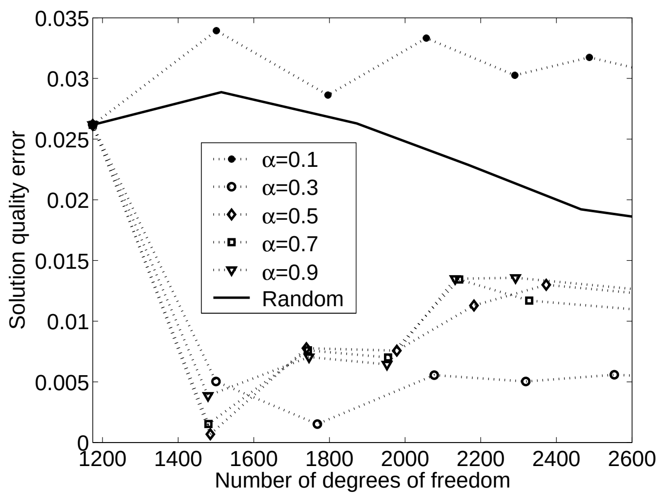

Fig. 6. Solution quality error vs. number of degrees of freedom for the waveguide through problem at $f = 10.5$ GHz. The all LT/QN number of degrees of freedom, at which the solution quality error is zero for all α, is 6836.

$\alpha \geq 0.5$ seems to be required.

A possible explanation for this tendency, which is also confirmed by inspection of the geometric distribution of the volume and face residual values, is as follows:

When a small enough number of elements are to be upgraded, exclusive use of the face residuals leads to the best results, because they are most effective in identifying the elements along the iris edge, where one would expect the greatest error in the approximate field representation to occur. It is well known that the electric field strength at such a re-entrant corner is singular and changes direction extremely fast in its vicinity [7]. The elements are of finite size and the polynomial orders of the basis functions are also finite, thus large inter-element discontinuities will be present as a matter of course. Away from the singularity, the variation in the true field is less intense and the volume residuals overshadow the face residuals in importance.

Figures 13 and 14 show the 2.5% elements with the largest error indicator values at $f = 9.5$ GHz, as identified by the $\alpha = 0.1$ and $\alpha = 0.9$ indicators respectively. Comparison of these two figures clearly shows the initial, superior capability of the $\alpha = 0.1$ indicator in identifying the elements along the iris edge in the middle of the waveguide.

From the performance graphs it can be seen via inspection that $\alpha = 0.5$ leads to the best all-round results for the waveguide iris problem. The value $\alpha = 0.5$ causes the relative solution quality error to decrease at a near optimal initial gradient in two out of three cases and leads to optimal relative solution quality error values at the highest upgrade percentage (12.5%) in all three cases.

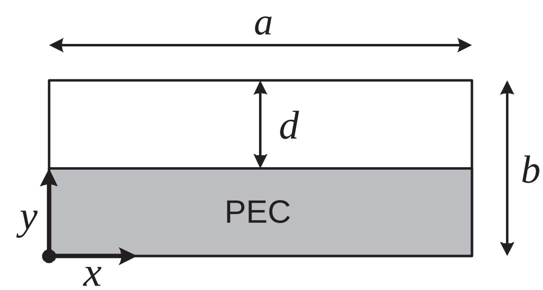

Fig. 7. Waveguide iris geometry. $a = 22.86$ mm, $b = 10.16$ mm and $d = 5.08$ mm.

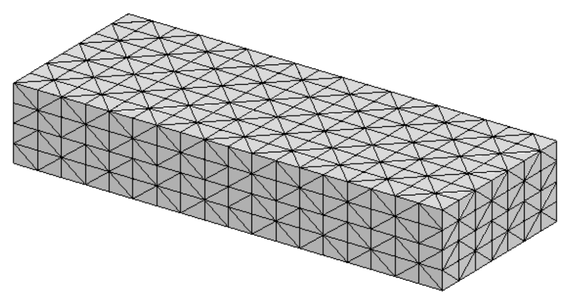

Fig. 8. Finite element mesh of the iris problem. 1889 elements, average edge length is 4.3 mm.

VII. Results: Performance Graphs of a Waveguide Bend Problem

This section considers a waveguide bend problem. The problem geometry is an E-plane, 90°, standard X-band, waveguide bend. Figure 15 shows the finite element mesh. Figure 16 compares the reflection coefficient values obtained with all-CT/LN- and all-LT/QN elements, with an approximate, analytical result by Marcuvitz [22], showing that the LT/QN result is indeed an improvement upon the CT/LN result. Again, [3] discusses the relevant manipulations of Marcuvitz's lumped-element model.

Performance graphs for this structure were calculated at $f = 8.5$ GHz, $f = 9.5$ GHz and $f = 10.5$ GHz. Figures 17, 18 and 19 show the performance graphs.

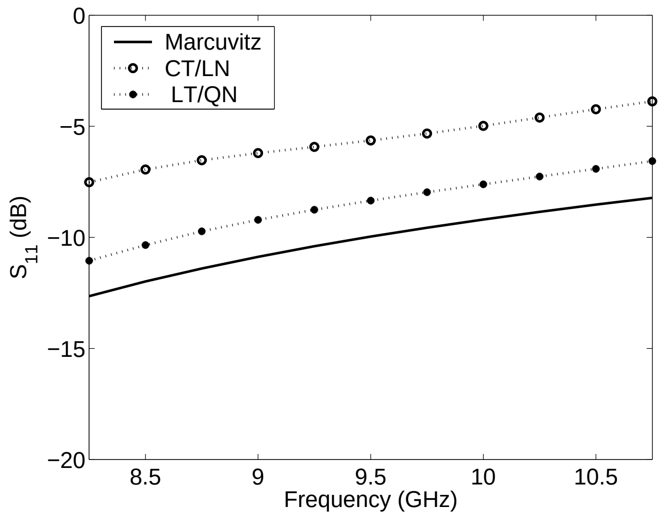

Fig. 9. S_{11} vs. frequency of the waveguide iris problem.

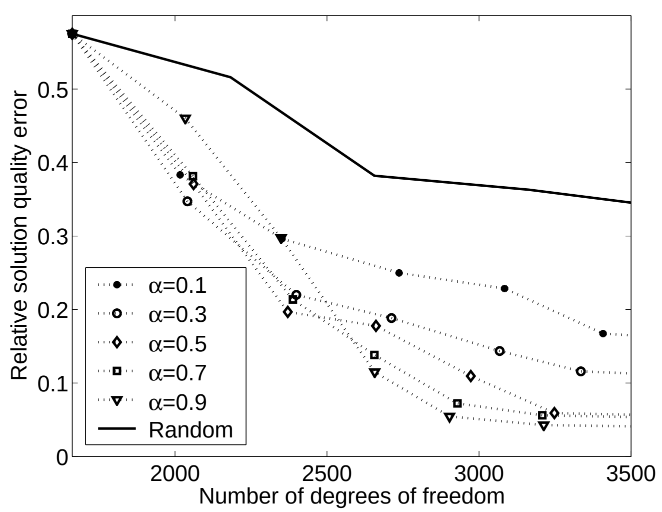

Fig. 10. Relative solution quality error vs. number of degrees of freedom for the waveguide iris problem at $f = 8.5$ GHz. The all LT/QN number of degrees of freedom, at which $\epsilon_Q = 0$ for all α, is 10144.

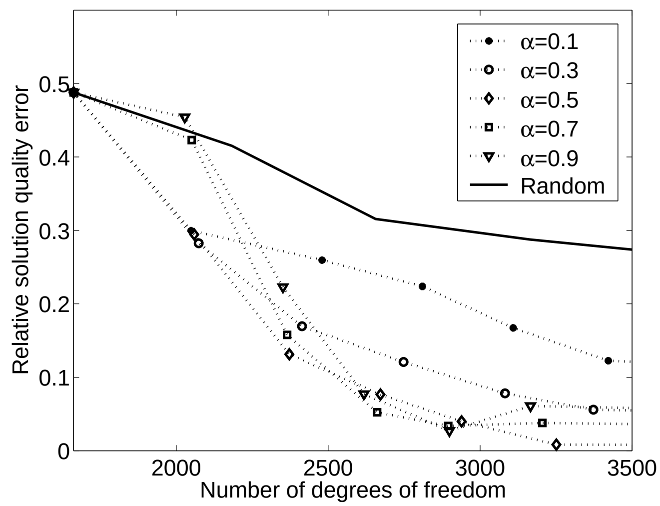

Fig. 11. Relative solution quality error vs. number of degrees of freedom for the waveguide iris problem at $f = 9.5$ GHz. The all LT/QN number of degrees of freedom, at which $\epsilon_Q = 0$ for all α, is 10144.

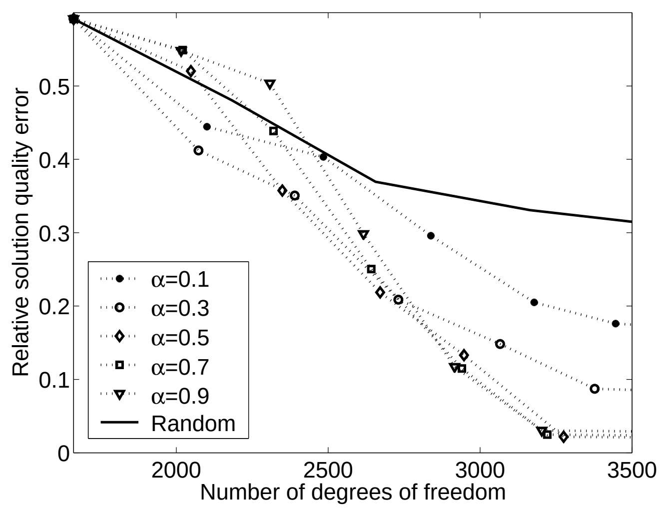

Fig. 12. Relative solution quality error vs. number of degrees of freedom for the waveguide iris problem at $f = 10.5$ GHz. The all LT/QN number of degrees of freedom, at which $\epsilon_Q = 0$ for all α, is 10144.

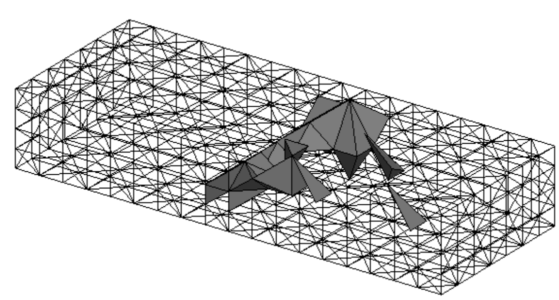

Fig. 13. The 2.5% elements with the largest error indicator values for the waveguide iris problem at $f = 9.5$ GHz, $\alpha = 0.1$.

Observe the following tendency in the performance graphs: throughout the range of degrees of freedom (upgrade percentages) considered, the $\alpha \geq 0.5$ indicators resulted in superior, near-identical performances in every graph.

The observed tendency is close to that of the waveguide iris problem in Section VI, except that at small upgrade percentages ($\leq 5\%$), the $\alpha \geq 0.5$ indicators remain superior to the $\alpha < 0.5$ indicators.

In the light of this similarity, we propose that the reason for the behaviour exhibited by the waveguide bend performance graphs are the same as that proposed for the waveguide iris problem's performance graphs. The difference in behaviour in the case of small upgrade percentages can be accounted for by noting that the field singularity at the re-entrant corner of the waveguide bend is of a lower order than that of the iris problem ($r^{-\frac{1}{3}}$ vs. $r^{-\frac{1}{2}}$, where r is a radial coordinate perpendicular to the re-entrant corner — see [23, p.178] for details). This means that the upgrade percentage below which the exclusive use of face residuals leads to superior results, is smaller than in the waveguide iris case. In fact, this percentage

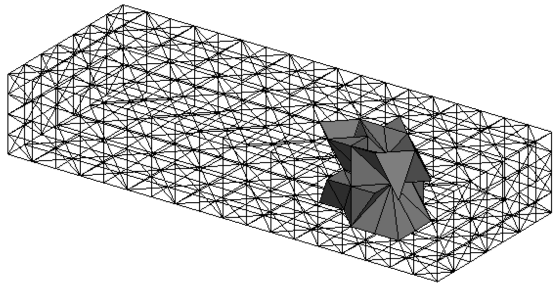

Fig. 14. The 2.5% elements with the largest error indicator values for the waveguide iris problem at $f = 9.5$ GHz, $\alpha = 0.9$.

is below 2.5% and thus, it is not shown in Figures 17, 18 and 19.

Figure 20 shows the 2.5% elements with the highest error indicator values in the case of $\alpha = 0.5$ and $f = 9.5$ GHz. Note how the re-entrant corner of the bend is covered, as one would expect (as motivated in Section VI for the iris edge).

As noted before within this section, $\alpha \geq 0.5$ leads to the best results for the waveguide bend problem.

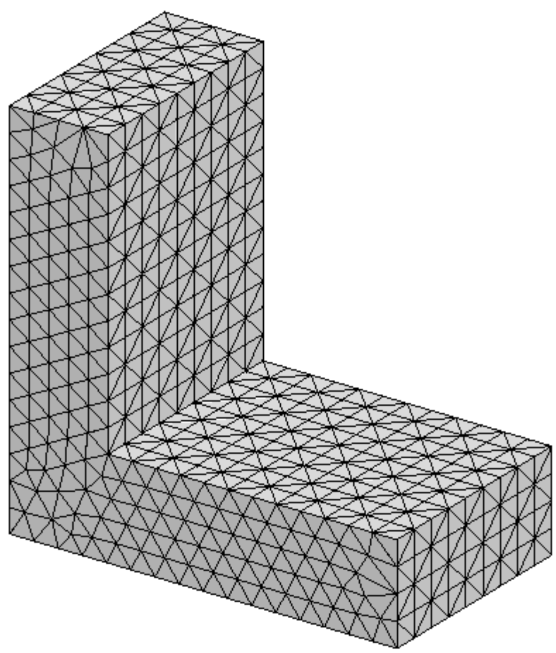

Fig. 15. Finite element mesh of the waveguide bend problem. 3331 elements, average edge length is 3.5 mm. The port geometries are as shown in Figure 1, with $a = 22.86$ mm and $b = 10.16$ mm.

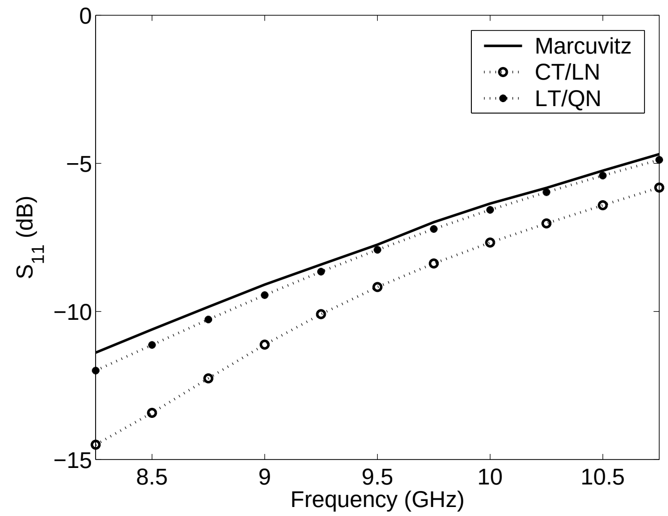

Fig. 16. S_{11} vs. frequency of the waveguide bend problem.

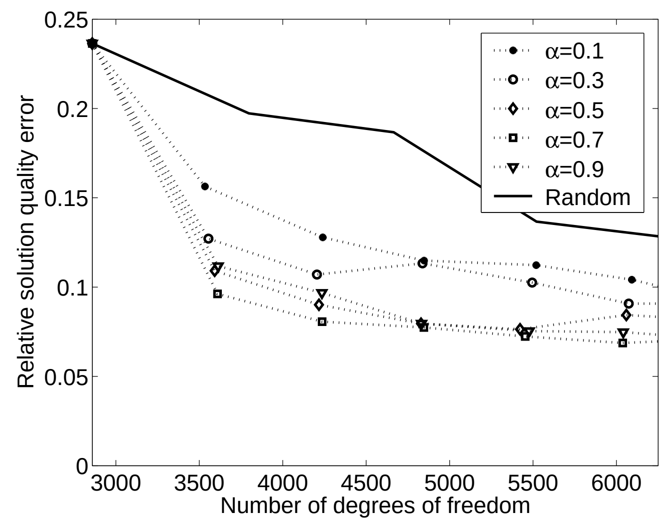

Fig. 17. Relative solution quality error vs. number of degrees of freedom for the waveguide bend problem at $f = 8.5$ GHz. The all LT/QN number of degrees of freedom, at which $\epsilon_Q = 0$ for all α, is 17628.

VIII. CONCLUSION

In this experimental investigation of an explicit, residual-based, a posteriori error indicator (presented in Section III) for driving a single level p-refinement of a related waveguide FEM formulation (presented in Section II), it seemed that the error indicator's performance is far superior to a benchmark, random selection, element upgrade scheme. The only poor results were encountered when considering the uniform, through problem, but as it is proposed in Section V, the through problem represents a special case that should be considered separately when evaluating the error indicator's general behaviour.

Though it was seen in Section VI that the face residuals may prove more important than the volume residuals in some regions and vice a versa, it is important to keep in mind that both residuals together are needed to form an upper bound on the approximate energy norm of the error field (see equation (11)), therefore they should both be present within a general indicator. This brings us to the choice of the parameter α in equation (18). Although it was found that the use of the indicator nearly always results in element selections that are superior to the random scheme, no matter the value of α, it does seem from the available results, that $\alpha \approx 0.5$ gives the most consistent results, but only marginally.

It was seen that the indicator considered here can be very effective; however, a couple of limitations should be kept in

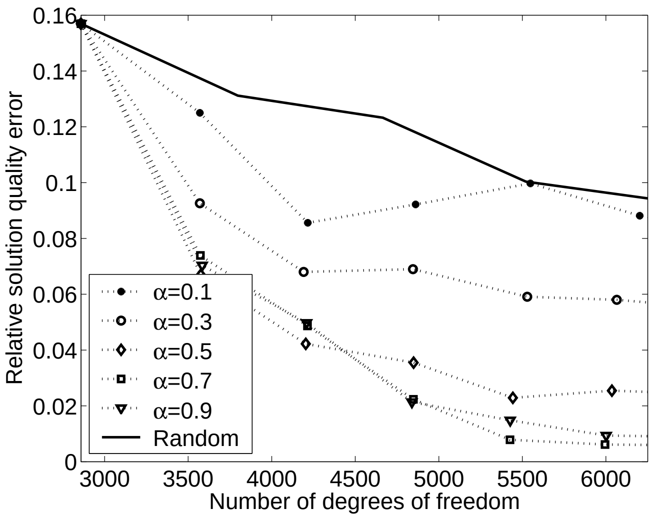

Fig. 18. Relative solution quality error vs. number of degrees of freedom for the waveguide bend problem at $f = 9.5$ GHz. The all LT/QN number of degrees of freedom, at which $\epsilon_Q = 0$ for all α, is 17628.

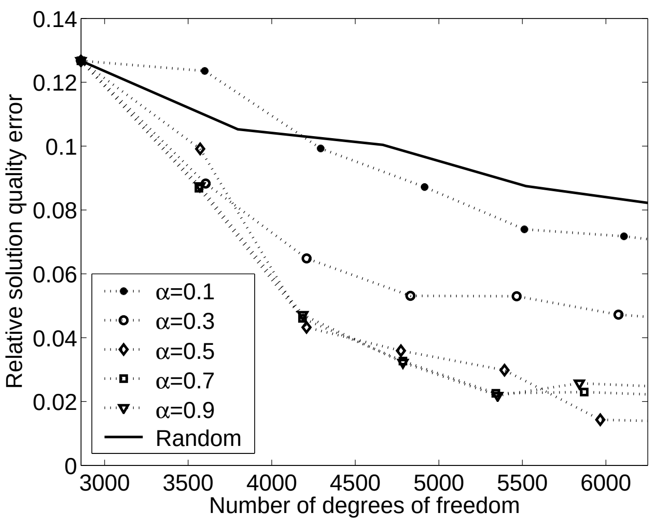

Fig. 19. Relative solution quality error vs. number of degrees of freedom for the waveguide bend problem at $f = 10.5$ GHz. The all LT/QN number of degrees of freedom, at which $\epsilon_Q = 0$ for all α, is 17628.

mind. Firstly, the error indicator only indicates relative error and not absolute error, which is a consequence of the unknown constants present within equation (11). This implies that it cannot be used as a termination condition of an iterative analysis procedure that guarantees a specified solution error bound. Secondly, the error indicator does not bound a proper norm of the true error and is therefore not guaranteed to perform consistently. Both of these limitations, which are inherently part of the indicator considered here, may possibly be overcome, to varying degrees, by considering other types of error indicators, error estimators and/or measures of the error.

Although not the topic of this present work, which has considered only the usual mixed-order elements, subsequent work has shown that for specific problems, full-order elements may be desirable. The waveguide iris problem is a good

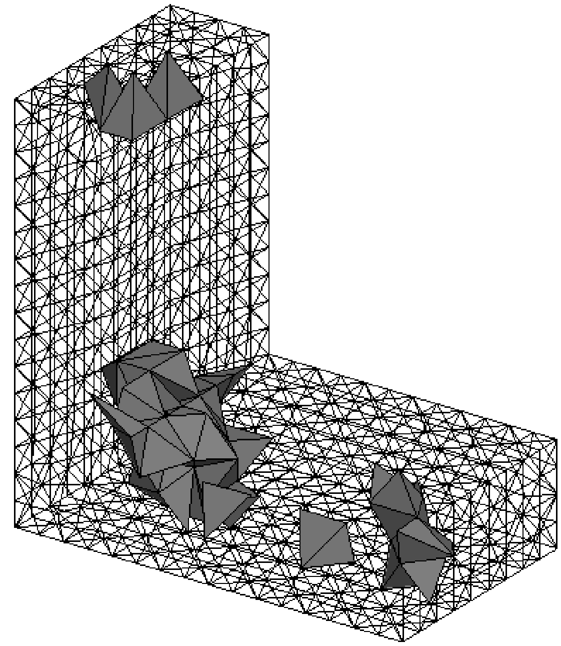

Fig. 20. The 2.5% elements with the largest error indicator values for the waveguide bend problem at $f = 9.5$ GHz, $\alpha = 0.5$.

example of such a structure. An extended discussion and results may be found in [24], and an adaptive scheme targeted specifically at such problems has been presented in [25]. A general adaptive scheme within which the error indicator discussed here could be employed, is presented in [26].

REFERENCES

[1] J.-M. Jin, *The Finite Element Method in Electromagnetics*, 2nd ed. New York: John Wiley and Sons, 2002.

[2] C. J. Reddy, M. D. Deshpande, C. R. Cockrell, and F. B. Beck, “Analysis of three-dimensional-cavity-backed aperture antennas using a combined finite element method/method of moments/geometrical theory of diffraction technique,” NASA, Langley Research Center, Tech. Rep. 3548, November 1995.

[3] D. B. Davidson, “Higher-order (LT/QN) vector finite elements for waveguide analysis,” *Applied Computational Electromagnetics Society Journal*, vol. 17, no. 1, pp. 1–10, March 2002, special Issue on Approaches to Better Accuracy/Resolution in Computational Electromagnetics.

[4] J. P. Webb, “Finite element methods for junctions of microwave and optical waveguides,” *IEEE Trans. Magn.*, vol. 26, no. 5, pp. 1754–1758, September 1990.

[5] J.-F. Lee, D.-K. Sun, and Z. J. Cendes, “Full-wave analysis of dielectric waveguides using tangential vector finite elements,” *IEEE Trans. Microwave Theory Tech.*, vol. 39, no. 8, pp. 1262–1271, August 1991.

[6] M. Salazar-Palma, T. K. Sarkar, L.-E. García-Castillo, T. Roy, and A. Djordjević, *Iterative and Self-Adaptive Finite-Elements in Electromagnetic Modeling*. Boston: Artech House, 1998.

[7] J. P. Webb, “Edge elements and what they can do for you,” *IEEE Trans. Magn.*, vol. 29, no. 2, pp. 1460–1465, March 1993.

[8] G. Mur, “Edge elements, their advantages and their disadvantages,” *IEEE Trans. Magn.*, vol. 30, no. 5, pp. 3552–3557, March 1994.

[9] A. F. Peterson and D. R. Wilton, “Curl-conforming mixed-order edge elements for discretizing the 2D and 3D vector Helmholtz equation,” in *Finite Element Software for Microwave Engineering*, T. Itoh, G. Pelosi, and P. P. Silvester, Eds. New York: John Wiley and Sons, 1996, pp. 101–125.

[10] M. M. Botha and D. B. Davidson, “An explicit a posteriori error indicator for electromagnetic, finite element-boundary integral analysis,” *IEEE Trans. Antennas Propagat.*, vol. 53, no. 11, pp. 3717–3725, November 2005.

[11] M. M. Botha, "Efficient finite element electromagnetic analysis of antennas and microwave devices: the FE-BI-FMM formulation and a posteriori error estimation for p adaptive analysis," Ph.D. dissertation, University of Stellenbosch, Stellenbosch, South Africa, December 2002.
[12] M. Ainsworth and J. T. Oden, "A posteriori error estimation in finite element analysis," *Computer Meth. in Appl. Mech. and Eng*, vol. 142, pp. 1–88, 1997.
[13] S. Polstyanko and J.-F. Lee, "Adaptive finite element electrostatic solver," *IEEE Trans. Magn.*, vol. 37, no. 5, pp. 3120–3124, September 2001.
[14] J. R. Stewart and T. J. R. Hughes, "A tutorial in elementary finite element error analysis: A systematic presentation of a priori and a posteriori error estimates," *Computer Meth. in Appl. Mech. and Eng*, vol. 158, pp. 1–22, 1998.
[15] P. Monk, "A posteriori error indicators for Maxwell's equations," *Jnl of Comp. and Appl. Math.*, vol. 100, pp. 173–190, 1998.
[16] K. K. Mei, "Unimoment Method for Electromagnetic Wave Scattering," *Journal of Electromagnetic Waves and Applications*, vol. 1, no. 3, pp. 201–222, 1987.
[17] S. Ramo, J. R. Whinnery, and T. van Duzer, *Fields and Waves in Communication Electronics*, 3rd ed. John Wiley and Sons, 1994.
[18] J. C. Nédélec, "Mixed finite elements in $\Re^3$," *Numerische Mathematik*, vol. 35, pp. 315–341, 1980.
[19] J. S. Savage, "Comparing high order vector basis functions," in *Proceedings of the 14th Annual Review of Progress in Applied Computational Electromagnetics*, March 1998, pp. 742–749, monterey, CA.
[20] P. G. Ciarlet, *The finite element method for elliptic problems*, ser. Studies in mathematics and its applications 4. Amsterdam: North-Holland, 1978.
[21] E. Kreyszig, *Introductory Functional Analysis with Applications*. New York: John Wiley and Sons, 1978.
[22] N. Marcuvitz, *Waveguide Handbook*. Peter Peregrinus, on behalf of IEE, 1986, originally published 1951.
[23] H. A. Haus and J. R. Melcher, *Electromagnetic Fields and Energy*. Englewood Cliffs, New Jersey: Prentice-Hall, 1989.
[24] D. B. Davidson, "An evaluation of mixed-order versus full-order vector finite elements," *IEEE Trans. Antennas Propagat.*, vol. 51, no. 9, pp. 2430–2441, Sept. 2003.
[25] M. M. Botha and D. B. Davidson, "A quasi-static condition for enhancing p-adaptive, mixed-order element, FE analysis," *Electromagnetics*, vol. 24, no. 1–2, pp. 13–24, January–March 2004.
[26] M. M. Botha and J.-M. Jin, "Adaptive finite element-boundary integral analysis for electromagnetic fields in 3-D," *IEEE Trans. Antennas Propagat.*, vol. 53, no. 5, pp. 1710–1720, May 2005.

Matthys M. Botha Matthys M. Botha was born in Stellenbosch, South Africa, 1976. He received the B.Eng. degree (cum laude) in 1998, in electrical and electronic engineering, and the Ph.D. degree in 2002; both from the University of Stellenbosch, Stellenbosch, South Africa. In January 2003, he joined the Center for Computational Electromagnetics, University of Illinois at Urbana-Champaign as a post-doctoral research associate, until September 2004, when he took up his present position as post-doctoral research fellow at the University of Stellenbosch. His primary research interest is in computational electromagnetics, with current focus on finite element and boundary element methods. He is a member of the IEEE.

David B. Davidson David Bruce Davidson was born in London, U.K., 1961. He received the B.Eng, B.Eng (Hons), and M.Eng degrees (all cum laude) from the University of Pretoria, South Africa, in 1982, 1983 and 1986 respectively, and the Ph.D. degree from the University of Stellenbosch, South Africa, in 1991.

Following national service (1984-5) in the then South African Defence Force, he was with the Council for Scientific and Industrial Research, Pretoria, South Africa, prior to joining the University of Stellenbosch in 1988. He is presently a Professor there. He was a Visiting Scholar at the University of Arizona in 1993, a Visiting Fellow at Trinity College, Cambridge University, England in 1997, and a Guest Professor at the IRCTR, Delft University of Technology, the Netherlands, in 2003.

He main research interest is computational electromagnetics (CEM), and he has published extensively on this topic. He is presently joint editor of the "EM Programmer's Notebook" column of the IEEE Antennas and Propagation Magazine. His first book, "Computational Electromagnetics for RF and Microwave Engineering", has been published by Cambridge University Press in 2005.

He is a member of the IEEE, ACES and SAIEE and is past chairman of the IEEE AP/MTT Chapter of South Africa. He is a recipient of the (South African) FRD (now NRF) President's Award.